




Impact Response of Polyurea Elastomeric Foams

P. Kauvaka¹ · M. Smeets² · B. Koohbor³ · G. Youssef¹ 

Received: 9 June 2023 / Accepted: 10 January 2024 / Published online: 24 January 2024
© Society for Experimental Mechanics, Inc 2024

Abstract

Providing effective protection from impacts in contact sports has been a foundation for the research of elastomeric cellular solids. Due to their superior energy absorption properties, polyurea elastomeric foams have emerged as a novel material candidate for impact mitigation in biomechanical and sports applications. This research utilized a small-scale shock tube to extend the application domain for polyurea foams to encompass higher strain rates. The experimental approach consisted of submitting foam plugs to a shock-propelled aluminum projectile with a velocity of ~ 24.5 m/s while capturing the impact event using high-speed imaging. The latter was analyzed using digital image correlation to extract the distribution of in-plane strain components in mono-density and density-graded foams. The density-graded samples were assembled using two interfacing strategies, namely adherent-free and thin layers of bulk polyurea adhesive. Experimentally measured strain-time histories revealed the effect of gradation and interfacing strategies at strain rates up to 4000 s⁻¹. The results affirmed that adherent-free, density-graded polyurea foams exhibited higher deformations than the adhered counterparts, even with relatively thin adhesive layers. In addition, polyurea foams developed a noticeable strain lag between the lateral and axial strains, exemplifying their hyper-viscoelastic behavior and improving energy absorption by broadening the strain-time peak. Most notably, polyurea foams, irrespective of the configuration, underwent reversible and momentary pseudo-liquefaction upon densification, reaching strains greater than 90%. This unique behavior indicates a new deformation mechanism for polyurea foams in sports applications where the foam rapidly conforms to the geometry of the impacted body, thereby shielding larger areas from violent impacts. All polyurea foam samples exhibited significant recovery within minutes, a promising attribute for greater impact efficacy in repeated loading scenarios.

Keywords Polyurea foams · Elastomeric foams · Impact loading · Protective padding · Digital image correlation

Introduction and Background

Elastomeric foams, capable of sustaining large, revisable deformations at a broad range of strain rates, are emerging as effective material candidates for protective gears in impact mitigation applications typical in contact sports.

In such loading scenarios, the protective padding endures force impulses within a few milliseconds; however, it has a significantly lower impact efficacy in subsequent loadings. Sports governing bodies (e.g., National Football League, NFL) recommend frequent replacements of the protective gears upon collision or impact to ensure player safety by avoiding accumulated damage and fatigue in the current state-of-the-art padding materials. Therefore, sports equipment made of novel, long-lasting elastomeric foams will potentially provide superior impact protection in single and multiple impact conditions, resulting in optimized safety for all participants at lower cost (reducing the need for frequent replacement) and weight penalties (using less and light materials) [1, 2]. Hence, pursuing lighter, impact-tolerant, and higher energy-absorbing foams is the overarching objective of this research vector.

Stochastic cellular solids (foams) are ubiquitous in sports protective gears, providing lightweight alternatives to their

P. Kauvaka, B. Koohbor and G. Youssef are members of SEM.

✉ G. Youssef
gyoussef@sdsu.edu

¹ Experimental Mechanics Laboratory, Mechanical Engineering Department, San Diego State University, 5500 Campanile Drive, San Diego, CA 92182, USA

² San Diego State University, 5500 Campanile Drive, San Diego, CA 92182, USA

³ Department of Mechanical Engineering, Rowan University, 201 Mullica Hill Rd, Glassboro, NJ 08028, USA

bulk counterparts, effective energy-absorbing and mechanical properties, and tunable attributes based on their densities [3]. Ethylene-vinyl acetate, polyurethane, expanded polystyrene, and expanded polypropylene foams are standard in helmets and their liners to provide comfort and impact protection. The mechanical performance of these foams has been vigorously investigated over the past few decades, elucidating their advantages and shortcomings [4–7]. Recently, polyurea foams have emerged as a viable alternative to the typical foams mentioned above, providing notable impact efficacy in single and repeated loading scenarios [1, 8–14]. Initially, polyurea foams were separately and concurrently reported by two research groups, including the current authors [13, 15, 16]. However, our group sustained assiduous research investigations, leading to this report [1, 8–10, 13, 14, 16–23]. Polyurea foams, synthesized based on aromatic polyurea, have been considered for several biomechanical and impact mitigation applications, including shoe insoles and football helmet liners at a broad range of strain rates, ranging from quasi-static to $<500 \text{ s}^{-1}$ [9, 11, 19]. While the primary outcomes of these research studies are summarized below, the overarching development is the superior and resilient mechanical and dynamic behavior of polyurea foams, attributed to their inherent hyper-viscoelastic constitutive responses [8, 13, 24, 25].

As mentioned above, the recent influx of experimental research on polyurea foams coincides with a patented green manufacturing process that solely relies on self-foaming and ambient curing without needing heat or vacuum [16]. Alternatively, Ramirez et al. reported another version of polyurea foams, where they controlled the rise of the foam in a heated vacuum environment [11, 12, 26]. Irrespective of the manufacturing process, polyurea foams have been vigorously studied for impact mitigation applications since aromatic bulk polyurea exhibits superior impact and shock-tolerant behaviors [27–30]. In essence, the desirable engineering properties of bulk polyurea were the primary motivators for pursuing foaming the same materials, translating these attributes to a lightweight cellular version [13, 16, 24]. Based on the patented manufacturing process of Youssef and Reed [16], polyurea foams are classified by a semi-closed cellular structure with native polyurea microspheres reinforcement [17, 18]. The semi-closed cell classification stems from the ubiquity of small perforations within the cell walls and the coexistence of small sealed cells [13]. Polyurea microspheres nucleate during the mixing process due to the polarity of the chemicals with respect to the deionized water based on precipitation polymerization, as later shown by Do et al. [17]. The microspheres are then preferentially deposited on the cell walls, providing additional reinforcement, as theoretically discussed in [17]. Reed et al. mechanically characterized 210 and 330 kg/m^3 polyurea foams and compared

their quasi-static and drop impact loading responses to an off-the-shelf benchmark foam [13, 31]. Under quasi-static loading, the high-density polyurea foam outperformed both the low-density and benchmark foams in absorbed energy [13]. The quasi-static responses were also used to calibrate an Ogden hyperfoam model, signifying the hyperelastic behavior of polyurea foams [13]. When subjected to moderate strain rates, the lower-density polyurea foam exhibited the highest reduction in acceleration despite being approximately 50% lighter than the benchmark foam [13]. Furthermore, it was concluded that polyurea foam can absorb up to 50% of the energy input while still making a full recovery and only losing 20% of its impact load-bearing ability upon repeated impacts [10]. Based on the results obtained from the aforementioned investigations, polyurea foams were considered in several biomechanical case studies, including helmet liners [11], shoe insoles [19], and padding protection for lateral falls [9], showing a remarkable potential in these applications.

The hyperelastic behavior of polyurea and elastomeric foams, generally characterized by large, reversible deformation, poses a significant experimental challenge in elucidating the mechanistic nuances associated with such large strain deformations. Hence, full-field strain measurement approaches, e.g., digital image correlation (DIC), have been used concurrently with mechanical loading at different strain rates to examine the multiscale deformation response of polyurea foams in conventional and density-graded configurations. DIC-coupled investigations linked the macroscopic mechanical responses to deformation underpinning in quasi-static and impact-loading scenarios [9, 23]. For example, full-field analysis assisted in reporting the time-dependent strain rates during impact loadings as a function of impact energy [1], exemplifying the hyper-viscoelastic response of polyurea foams [10]. Notably, the strain rate was found to be nonuniform throughout the loading event, peaking at the onset of the impact, which was mildly dependent on the input impact energy [1], given the strain rate sensitivity of this type of material [14]. The DIC-measured strain rates developed in polyurea foams exemplified their optimal utility for low-velocity (low-energy) impact scenarios, attenuating the force and broadening the impulse duration [1]. Furthermore, DIC analyses of polyurea foams submitted to repeated impacts suggested that internal damage (also confirmed by electron microscopy) could be associated with a slight decrease in their impact mitigation efficacy. The strain contour maps indicated heterogeneous strain distribution due to localized deformation fields, leading to local damage and a tendency toward quasi-auxetic behavior [10]. Finally, DIC analyses bridged the length scale between micro and macroscopic behaviors, showing

that the transition length is a function of material density but independent of global strains [32].

With an emphasis on density gradation strategies, Uddin et al. studied the mechanical response of density-graded polyurea foams, investigating the effect of ~1 mm thick adhesive interlayers on the mechanical performance under quasi-static and dynamic loading conditions [21]. Uddin et al. demonstrated the effect of adhesive layer stiffness on the energy dissipation performance of polyurea foams, where a mechanically compliant adhesive improved the energy dissipation efficiency [21]. Inspired by the outcomes of the latter study, Smeets et al. challenged the interfacial strategies in density-graded elastomeric foams, e.g., polyurea foams, reporting the difference in the mechanical performance of bilayer and trilayer foam structures under quasi-static and dynamic loading conditions [9, 23]. Smeets et al. assembled the density-graded foams using the natural adhesiveness of the foam slurry and the strong adhesive properties of bulk polyurea, resulting in seamless and thin adherent interfaces, respectively [9]. Under quasi-static loading, the results showed that each configuration excelled in different performance metrics, where the monolayered polyurea foam exhibited the highest specific energy absorption [9]. Similarly, the mono-density polyurea foam reported the largest specific energy absorption under the impact, outpacing the density-graded counterparts due to the low gradation distribution and incoming impact energy [23]. Hence, another motivation for this research is to probe the deformation performance of density-grade polyurea foam structures at higher impact energies.

The research leading to this report aimed to elucidate the impact efficacy of density-graded polyurea foams in high-speed loading scenarios while comparing the performance of two control groups. As mentioned above, this research is motivated by pursuing novel, density-graded foams with elastomeric properties capable of potentially sustaining multiple impacts congruent with sports applications. However, there needs to be more understanding of the mechanics of elastomeric foams under high-velocity impacts, including the deformation mechanisms throughout the impact event and post-impact recoverability. The density-graded samples were fabricated in-house into bilayer and trilayer structures using two interfacial strategies, namely “seamless” based on the natural adhesiveness of the foam slurry and “adhered” using bulk polyurea to bond separately pre-fabricated sheets with varying densities. The control groups consisted of mono-density polyurea and benchmark foams. Square cuboid samples were extracted and submitted to impact loading by releasing an aluminum projectile from a shock tube while collecting high-speed images for post-loading DIC analyses. The novelty of this research hinges on reporting a quasi-liquefaction phenomenon, the first time

observed in elastomeric foams under direct impact loading, with remarkable recoverability of polyurea foams, irrespective of gradation or interfacial strategies. Previous research focused only on the response of elastomeric polyurea foams under impact velocities < 5 m/s, evading the liquefaction phenomenon due to the limited impact energy. The momentary pseudo-liquefaction improves the conformability of the foam padding, resulting in activating additional energy shunting mechanisms.

Materials and Methods

Materials and Samples Preparation

Density-graded polyurea foam samples were manufactured in two configurations, including positively graded bilayer and trilayer structures, where positive gradation indicates the lowest density foam layer faces the impacting projectile. In contrast, the highest-density layer is located on the opposite side [33]. Positive gradation, where the lighter density foam faced the projectile, is considered herein since it provides sequential deformation to manage the impact forces effectively. In other words, the lighter-density foams undergo large deformation, maximizing the strain energy and leading to the engagement of the consecutive layer with higher relative density in the overall mechanical response. The square cuboid samples were extracted from 30 cm × 30 cm sheets produced using a modified mold casting process previously reported in [9]. The focus here is on discrete gradations by only considering bilayer and trilayer foam configurations, given the current limitations of manufacturing and assembly procedures. Future reports will explore the mechanics of continuously graded polyurea foams under a broad range of strain rates. For completion, the foam manufacturing process is briefly summarized herein, but the reader is referred to [16] for additional details on this patented manufacturing technology. The foam sheets were cast in Teflon-coated aluminum mold with the desired geometry, where a frothed polyurea foam slurry was poured to a specific mass such that the volume of the mold cavity and the pour mass dictated the final foam density. The frothed foam slurry was prepared by mechanically mixing modified methylene diisocyanate (Isonate 143 L MDI, Dow Chemical) and oligomeric diamine (Versalink P1000, Evonik) in deionized water at a weight ratio of 1:4, respectively. Before pouring the foam slurry, the excess water was drained by cutting a slit at the bottom of the mixing container to avoid unintentional water pockets within the final foam sheet. The foam sheets were cured for 24 h in the covered mold and an additional 48 h after de-molding for dehydration and final curing. All curing steps were performed in ambient conditions without

heat or vacuum, marking the advantages of this manufacturing process, as explained previously in [16]. As discussed in the forthcoming sections, foam plugs were removed from the cured sheets and mechanically characterized using projectile impact from a shock tube and high-speed imaging. Before testing, the geometrical and gravimetric attributes of the samples were cataloged and archived based on three specimens extracted from each configuration.

The abovementioned manufacturing process was further extended and modified to fabricate density-graded foam sheets. In one variation, sequential casting was used to create seamless interface bilayer and trilayer foam sheets, relying on the natural adhesive properties of the uncured foam slurry and the excellent adhesiveness of bulk polyurea [34]. To cast a bilayer density-graded foam, an initial sheet was manufactured and cured, as discussed above, followed by a second pour by systematically adjusting the dispensed mass and the volume of the mold cavity. Notably, no additional steps were taken before pouring the second layer, leaving the original surface of the first foam sheet in pristine conditions, resulting in a seamless interface since the frothed foam slurry penetrated the open pores and locked onto the existing surface pores. Smeets et al. recently provided micrographic evidence based on scanning electron microscopy of the resulting interfaces [9]. Then, a third layer was cast faithfully following the same process to create seamless interface trilayer foam sheets with positive gradation. In an alternative approach, individual foam sheets were prefabricated using the mold casting process, where the density of each sheet also varied by changing the dispensed mass and the mold volume, as discussed above. Once the sheets were completely cured, a thin layer of bulk polyurea (prepared using the same chemicals and ratios reported before) was spread on the exposed surface using a simplified doctor blade method, resulting in an ultrathin adhesive layer, ca. 5 μm [9]. The assembled bilayer foam structure was placed between two rigid plates under 22 kPa static pressure for 36 h for the adherent polyurea layer to set fully, avoiding shifting or early debonding. The same adhesion process was followed to create a trilayer foam configuration. In all, two interfacing approaches were used to prepare bilayer and trilayer foams, namely, seamless and adhered interfaces.

Table 1 lists the foam configurations investigated herein, including respective densities and dimensions.

In addition to the density-graded samples, two sets of square cuboid mono-density polyurea foam samples and off-the-shelf reference foam were extracted from prefabricated sheets. The mono-density samples acted as control groups to benchmark the impact-induced deformations of their density-graded counterparts. The choice of mono-density polyurea foam is rationalized to delineate the effect of the seamless interface on the strain state, as discussed next. On the other hand, the off-the-shelf reference was opted in since it is advertised as the ‘gold standard’ in impact mitigation at moderate and impact loading scenarios [31]. The benchmark foam is based on a proprietary chemical formulation and is ubiquitous in mitigating high-velocity impacts such as motorcycle accidents. The front (camera-facing) surface of each cuboid sample, irrespective of interfacing approach or density-gradation, was coated with surface speckles in greyscale shading to accommodate concurrent, high-speed imaging and DIC analyses, as discussed next.

Experimental Methods

Figure 1 shows the built-in-house, instrumented shock tube used in the high-speed impact loading of all foam samples. The shock tube loading mechanism consists of a compression chamber (driver section) separated from the low-pressure driven section by a thin polymer buffer (Skyrol® SW84G, Curbell). The thin buffer was clamped between two steel flanges connecting the driver and driven sections of the shock tube. A pre-calibrated piezoelectric pressure sensor (ICP® 102B06, Piezotronics) was mounted close to the muzzle, consisting of a projectile holding flange and short tube, as shown in Fig. 1. The piezoelectric sensor was connected to a digital oscilloscope (MDO3102 Tektronix), which was self-triggered based on the shock front pressure signal, acquiring the shock profile during each loading step. The small-scale shock tube consistently produced a shock front pressure of 85.7 ± 4.42 kPa. The during-loading shock attributes were compared to the unmuzzled counterpart to contrast the differences due to the presence of an aluminum projectile. The projectile was a ~200 g aluminum slug with

Table 1 Summary of sample configurations and their associated gravimetric and geometric attributes

Sample Configuration	Density (kg/m^3)				Height (mm)			
	ρ_I	ρ_{II}	ρ_{III}	ρ_{eff}	H_I	H_{II}	H_{III}	$L_{overall}$
Benchmark (B)	397 ± 2	-	-	397	16.74	-	-	16.74
Monolayer (M)	255 ± 5	-	-	255	17.25	-	-	17.25
Seamless Monodensity (SM)	292 ± 9	294 ± 11	-	293	7.10	11.44	-	18.54
Seamless Bilayer (SB)	287 ± 6	332 ± 25	-	311	9.42	10.49	-	19.91
Adhered Bilayer (AB)	253 ± 4	309 ± 1	-	281	10.32	9.62	-	19.94
Seamless Trilayer (ST)	234 ± 2	248 ± 6	273 ± 7	252	8.31	8.83	7.62	24.76
Adhered Trilayer (AT)	231 ± 5	253 ± 4	309 ± 1	265	9.50	10.64	9.24	29.38

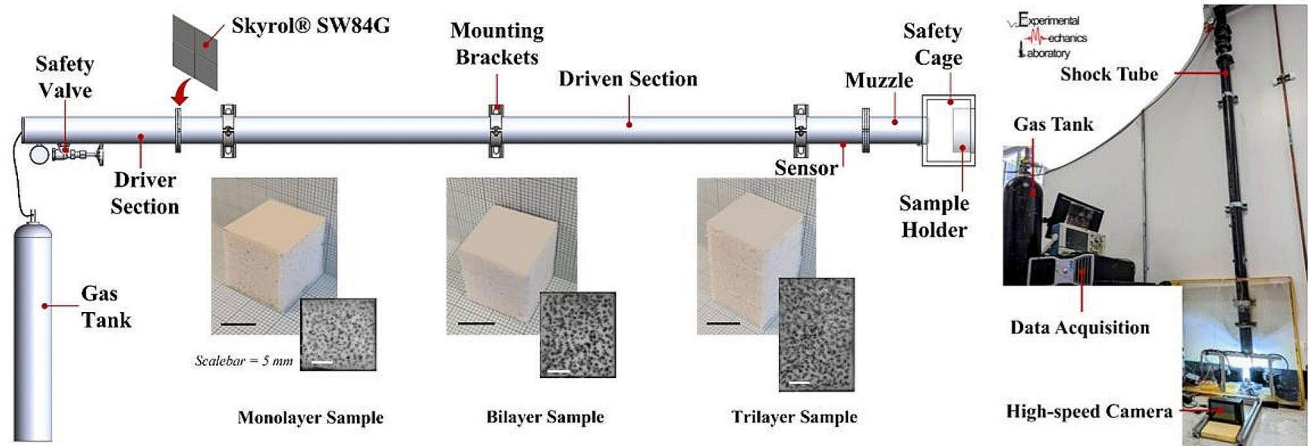


Fig. 1 (a) Schematic representation of the experimental setup, including the shock tube, the sample platform, the protective acrylic cage, and the electronics with a pictorial collage of the specimens submitted

to impact loading, including monolayer, bilayer, and trilayer polyurea foam samples. (b) A picture of the physical setup used in this research

a flat front to load the foam samples uniformly at an impact velocity of ~ 24.4 m/s, determined from tracking the projectile surface before contact with the sample. The dimensions of the aluminum projectile are 50.80 mm ID, 63.50 mm OD, and 57.15 mm tall. The impact velocity was determined by tracking the projectile position once it exited the shock tube until contacting the sample and the time elapsed during this journey. The selection of the impact velocity hinges on previous biomechanics investigations in action and contact sports, exceeding 10 m/s in combat sports [35], e.g., kick-boxing, and 30 m/s in cricket [36], to name a few examples [37, 38].

The samples were saddled on a steel platform using double-sided tape to avoid unintended motion during field-of-view optimization and uncontrolled ejection after impact. The projectile was suspended at the onset of the muzzle section using two permanent magnets since the shock tube was mounted upright for space economics and safety precautions (launching the projectiles toward the ground). Two permanent magnets were symmetrically attached to the projectile walls, holding the aluminum slug into place. The projectile was released upon rupturing the buffer film and the arrival of the generated shock front to the muzzle section. The latter was contained within a transparent acrylic cage to house the accelerated projectile and the illumination source accompanying the high-speed photography using a digital camera (Fastcam SA 1.1, Photron) fitted with a NIKKOR 72 lens. Since the small-scale shock tube can cause permanent deformation that could convolute the resolved strain data, each sample (three from each configuration) was tested once to circumvent the fatigue and internal damage effects. The digital images were acquired at a rate of 30,000 fps, covering the entire surface of the sample at an image size of 416×384 pixels. The photos were separately analyzed using

commercial digital image correlation software (Istra 4D, Dantec Dynamics) and image analysis software (ImageJ, National Institutes of Health). The DIC analysis used engineering strain formulation and a subset-based local DIC correlation algorithm [39]. The DIC software tracks the facets, measuring the displacements and strains using the local deformation of a single facet. A Supplementary Video captures the impact event of the polyurea foam sample in the conventional monolayer configuration to assist in the visualization of the resolved deformations and strains discussed in the forthcoming sections. It is worth noting that the results discussed in the upcoming sections are based on 2D DIC analysis since only one high-speed camera was available and used. Therefore, only the in-plane strains were resolved, including the longitudinal strains along the height of the sample (the y -direction) and the transverse strain along the width of the sample (the x -direction). The facet size was adjusted between 21 and 29 pixels, and the grid spacing ranged between 9 and 13 pixels based on the sample configuration while keeping the search radius constant at 10 pixels. The relative humidity and enclosure temperature were recorded during testing (HTM-238, Gain Express), while the sample temperature was measured using a thermocouple (USB-TC01, National Instruments) mounted close to the surface to report any temperature variation due to the intense illumination and violent impacts.

Results and Discussion

At the onset, it is imperative to discuss the speckle pattern greyscale intensity distribution since the overall performance of the image analysis algorithm hinges directly on distinguishable speckles throughout the correlation,

especially at maximum compression, as discussed next. The speckles were created using multicolor permanent markers bundled together to apply random patterns on the surface of the samples, achieving a broad range of greyscale shading. Figure 2 includes three sub-panels reporting the histograms of the greyscale distribution (0 \diamond black and 255 \diamond white) from three representative samples, signifying the range of grey shades based on the contrast resulting from the speckling process and the natural color of the foam. Notably, the natural color of polyurea foams is ivory (corresponding to ~ 200 on the greyscale), while the benchmark foam has an orange appearance (~ 240 on the greyscale). Figure 2a is the histogram of the surface of a bilayer polyurea foam sample. Figure 2b and c represent the histograms from monolayer polyurea and benchmark foams, respectively. The histogram in Fig. 2a shows a broad distribution of greyscale, nearly encompassing the entire greyscale range, that is slightly skewed towards the white shade due to the natural ivory color of polyurea. Figure 2b, the histogram of the monolayer polyurea foam, is limited to shades < 200 , implying that the combined effects of speckling and illumination nearly obscured the natural appearance of the sample. The histogram in Fig. 2b is generally centered despite the absence of shades corresponding to the natural color of the sample. Upon full compression, the speckles merged, negatively affecting the contrast and resulting in de-correlated areas in the fully compressed samples. The quality of the speckles was also compromised due to excessive out-of-plane motion stemming from the hyperelastic response of elastomeric foams. Finally, Fig. 2c shows that the intensity distribution in the benchmark is skewed toward white; however, the image correlation process remained unaffected since these samples did not reach full densification. The greyscale distribution on the surface of the specimens tested herein was iteratively optimized for the current experimental setup, accounting for the limitations of available lighting

sources and resolution of the imaging system. The informal speckle optimization process entailed using sacrificial samples to tune the shading distribution by iteratively speckling, testing, and analyzing until the pattern and distribution used herein were achieved.

Figure 3a is a schematic representation of the virtual line and area gauges used to extract the strain within a specific region, including the overall average, individual layers within the graded structures, and across the interface areas. Notably, the strain within individual layers and over the entire sample surfaces was resolved using area gauges, while line gauges were used to track the interface deformation. Figure 3b summarizes the average strain rates ($\dot{\epsilon}$) in each sample configuration, corresponding to the maximum resolved strains. The induced dynamic impact response reported herein was based on the sudden release of the aluminum projectile due to a 2 atm difference in the pressure at the shock front (measured from an unmuzzled shock tube) based on the rupture of the thin plastic buffer. Figure 3b shows the nominal strain rate in each layer for the bilayer ($\dot{\epsilon}_I$ and $\dot{\epsilon}_{II}$) and trilayer ($\dot{\epsilon}_I$, $\dot{\epsilon}_{II}$, $\dot{\epsilon}_{III}$) density-graded polyurea foam structures. The rate was calculated by tracking the strain using a linear gauge, extending over the longitudinal direction of the masked region of interest or within each layer for the graded structures. Additionally, Fig. 3b reports the strain rate across the interface regions. The strain rate was then resolved using the finite difference method to differentiate the longitudinal strain with respect to loading time. Notably, the resulting strain rate values were not filtered or smooth since the results were smooth for rate extraction. The results in Fig. 3b indicate the highest achieved strain rate of $\sim 1900 \text{ s}^{-1}$ for the benchmark foam, followed by monolayer polyurea foam at a strain rate of $\sim 1600 \text{ s}^{-1}$. The lowest reported average strain rate of $\sim 830 \text{ s}^{-1}$ for the adhered trilayer polyurea foams, accounting for the axial deformations along the sample, including

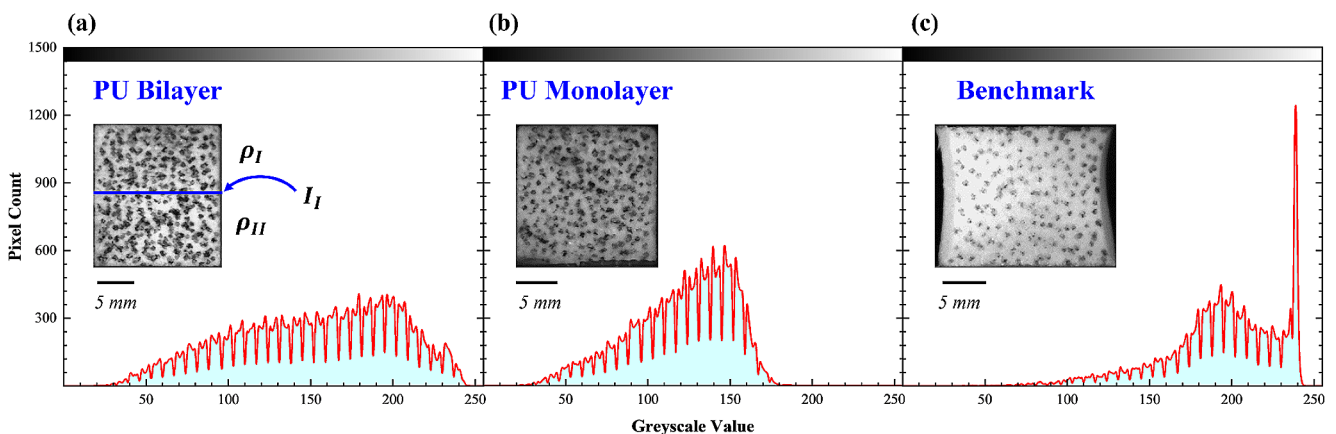


Fig. 2 Representative histograms from three samples to show the contrast distribution based on the natural color of the materials, the illumination, and speckle pattern from (a) benchmark, (b) polyurea monolayer, and (c) polyurea bilayer foam samples

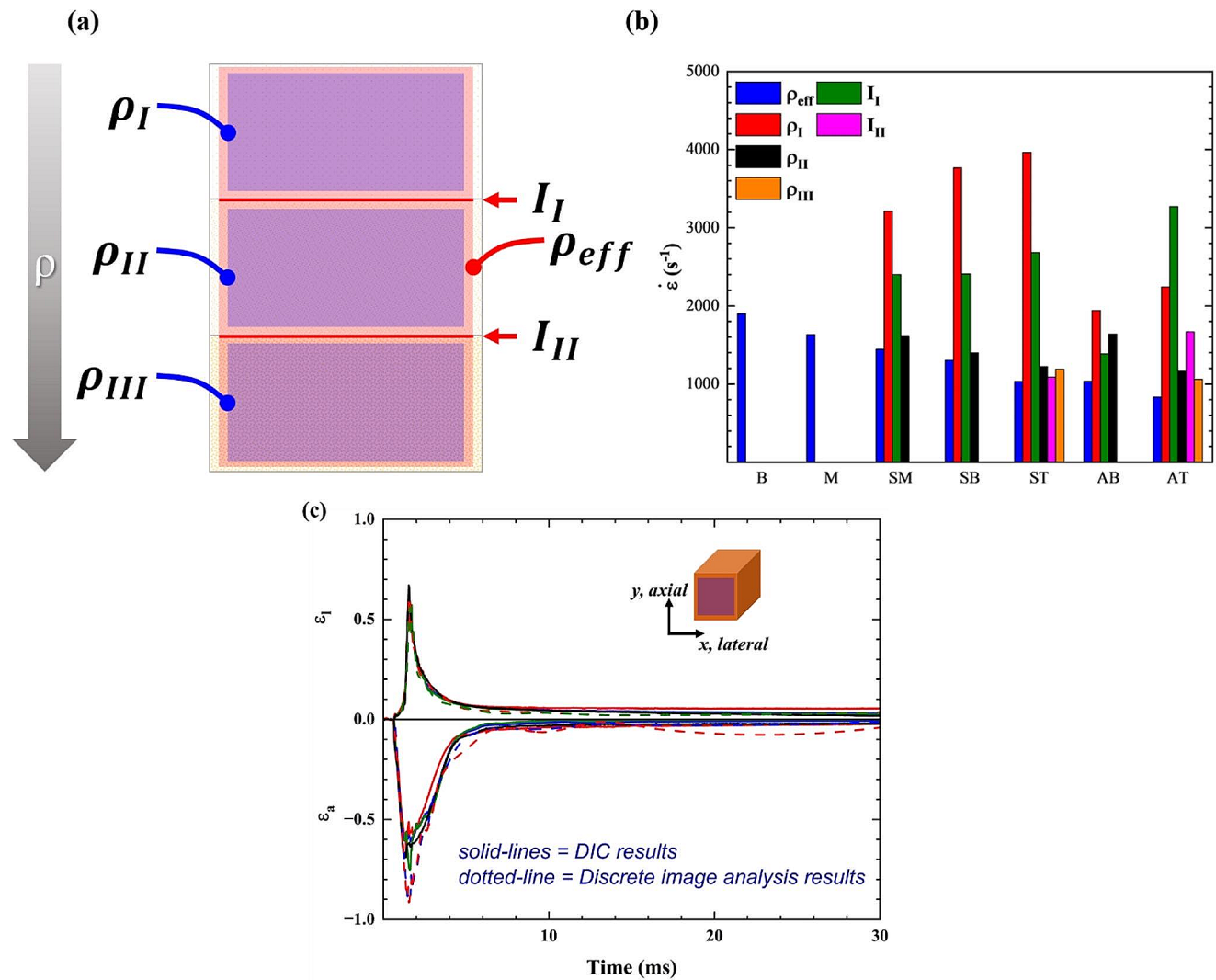


Fig. 3 (a) Schematic of the density-gradation strategy and the virtual strain gauges used in this research, including area gauges for strain tracking with individual layers and line gauges at the interfaces. (b) Maximum strain rate recorded from all sample configurations, includ-

ing the strain rates within each individual layer and across the interfaces of multilayer density-graded samples. (c) Comparison of the axial and lateral strains from the seamless mono-density samples extracted from DIC and discrete image analyses, showing good agreement

the three density-graded layers and two interface regions, schematically represented in Fig. 3a. Generally, the average strain rate is inferior to that of individual layers since the averaging process implies smearing the data throughout the sample height as the projectile decelerates to generate maximum compression. The dichotomy of the average strain rates also stems from the time-dependent properties (e.g., strain rate sensitivity and viscoelasticity) of the base materials used in polyurea and the benchmark foams.

The strain rate results in Fig. 3b reveal two additional observations: the strain rates of the individual layers and interface regions. Axiomatically, the emphasis here is on bilayer and trilayer polyurea foams that were positively graded such that the lowest foam layer was facing the incoming projectile. In this case, the lowest density layer

(top layer) reported the highest strain rates, $\sim 4000 \text{ s}^{-1}$ for the seamless trilayer structure and $\sim 3800 \text{ s}^{-1}$ for the bilayer counterpart. Notably, the effective density of the former is 234 kg/m^3 while the latter is 287 kg/m^3 , indicating the density played a secondary role in the generated strains within the top layer. Based on Gibson and Ashby scaling laws, the relatively low density of the top layer facing the projectile indicates higher mechanical compliance [5], yielding large and faster deformation, i.e., impact loading at a higher reported strain rate. Instead, the strain rate of the first layer primarily correlated with the interfacial strategy such that the adhered interfaces resulted in significantly lower strain rates, ca. 22% on average, than those reported in the presence of the seamless interface. Density-graded structures with seamless interfaces were recently shown to

homogenize the effect of discontinuities between two layers since the foam slurry could penetrate the surfaces of the previously cured foam sheet, providing additional mechanical interlocking and increasing the interface resistance to deformations [9]. On the other hand, bulk polyurea adherent ($\sim 5 \mu\text{m}$) [9] resulted in a notable decrease in the strain rate of the capping layer, which is desirable in impact mitigation applications. It is imperative to note that the shock conditions resulting in launching the projectile toward the samples were nearly identical, further supporting the presumption of the favorable effect of adhered interfaces on the impact efficacy of density-graded elastomeric foams. Overall, the reported strain rates in Fig. 3b represent a multi-fold increase over those previously reported in [1, 8–10, 12–14, 21–23], signifying the favorable influence of density-gradation in impact mitigation applications at moderate strain rates. Future research will explore the extent of the effect of strain rates on the impact efficacy of density-graded elastomeric foams.

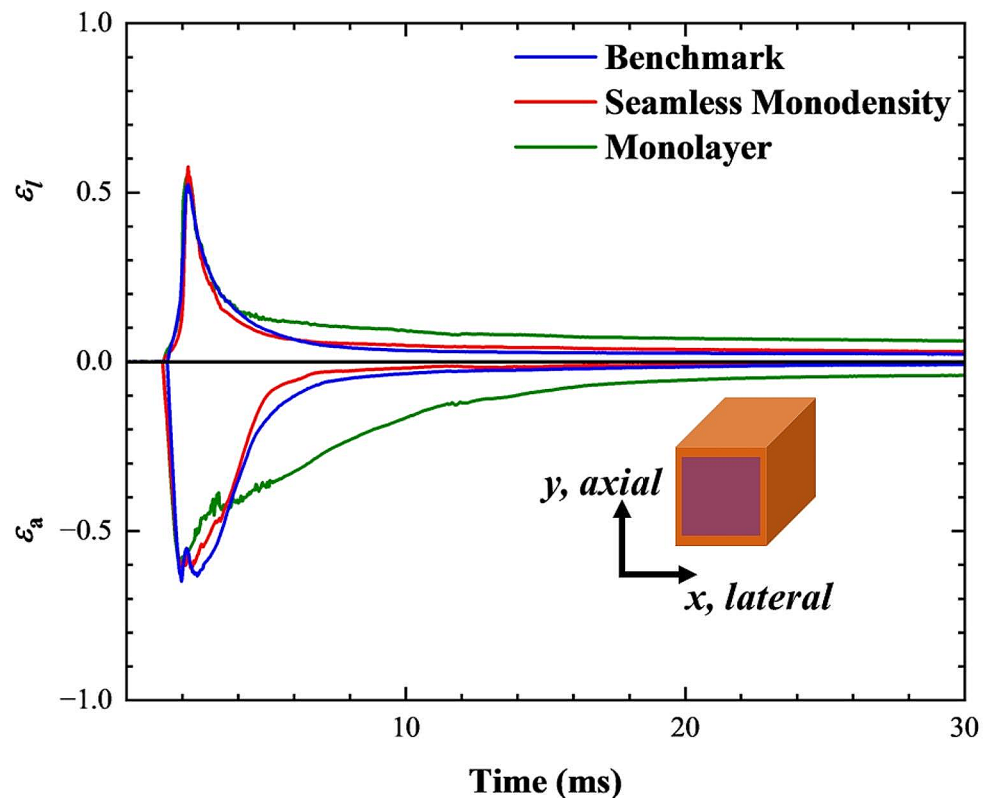
Another notable observation from Fig. 3b is the relative values of the strain rates within the first interface regions compared with the rate performance of the top layer that has the lowest density within each bilayer and trilayer graded structure. The strain rate in the first interface region for the seamless sample configurations, irrespective of the number of layers, was found to be $\sim 3700 \pm 320 \text{ s}^{-1}$ based on the average values from the seamless mono-density, seamless bilayer, and trilayer samples. The similarity of the strain rate within the interface region separating the first and second layers, regardless of the density variation and total number of layers in the graded foam structures, is attributed to the consistency of interface quality of seamlessly assembled samples. In such cases, the interface is formed naturally and slowly based on the adhesive properties of the uncured polyurea slurry, which can also penetrate the cellular microstructure on the surface of previously fabricated sheets. Since the foundational foam sheets were never removed from the mold and the surfaces remained pristine, it promoted consistent chemical and mechanical interfacing mechanisms that highlighted the strain transition within the first interface region distinctively. On the other hand, the adhered samples, e.g., adhered bilayer and trilayer polyurea foams, showed a significant variation in the strain rate values, ranging from $\sim 1400 \text{ s}^{-1}$ for the former to $\sim 3300 \text{ s}^{-1}$ for the latter. The substantial dichotomy in the interface region strain rate is potentially attributed to the variation in the adhesive thickness and coverage since it was applied manually.

Before discussing the DIC results, Fig. 3c compares the resolved strains using digital image correlation (Istra 4D) and discrete image analysis (ImageJ analysis of individual images). The results affirm that the DIC is reliable, and the setup and analysis approach summarized in the previous

section are repeatable and accurate. Figure 4 summarizes the in-plane strain components in the foam samples with single density throughout, including two variations of polyurea foams (e.g., monolayer with $\rho = 255 \pm 5 \text{ kg/m}^3$ and bilayer with $\rho_I = 292 \pm 9 \text{ kg/m}^3$ and $\rho_{II} = 294 \pm 11 \text{ kg/m}^3$) and the benchmark counterpart ($\rho = 397 \pm 2 \text{ kg/m}^3$). The results in Fig. 4 compare the axial (along the impact direction) and lateral (transverse to the loading direction) strains within these conventional foam configurations, i.e., ungraded. While the lateral strain initially tracked their axial companion during the rise time for the benchmark foams, indicating temporary suppression of the time-dependent behavior, there was a notable lag between the lateral and axial strains in polyurea foams. The lateral strain-time histories of polyurea foams exhibit an initial knee despite the sudden increase in the axial strains generated upon contact between the projectile and the samples. The temporal trailing of lateral strains in polyurea foams elucidates their hyper-viscoelastic properties. It gives rise to additional energy dissipation mechanisms, such as shunting the energy away from the impact structure. Upon full compression and reversal of the direction of the projectile motion, the lateral strains recovered asymmetrically and relatively faster than their axial strain counterparts, indicating directional anisotropy since the lateral directions were unconfined. At the same time, the samples had to bear the projectile axially until complete departure. It is, however, imperative to note that polyurea foams recovered slower laterally than the benchmark foam since the latter is closed-cell foam, where the entrapped and compressed air accelerated the lateral recovery. Full recovery was imminent in benchmark and bilayer polyurea foams but sufficiently delayed beyond the analysis time in the monolayer polyurea foam samples.

Overall, the performance of ungraded polyurea and benchmark foams appears similar, irrespective of the material or density. This can be attributed to the high energy impact resulting in high strains up to full densification. These similarities also stem generally from the waveform characteristics, including amplitude and spread. However, further comparison between polyurea and benchmark foams indicates that three subtle differences are noteworthy. First, polyurea foams were less dense than the benchmark counterparts, but the in-plane strain-time histories of the bilayer polyurea and the latter are nearly identical. That is, polyurea foams endured significant strains at a lower weight penalty, which is imperative for developing the next generation of protective sports gear, e.g., effective and lightweight. Second is the recovery spread of the axial strain associated with the monolayer polyurea foams extending $> 15 \text{ ms}$ beyond the recovery of the remaining samples. In other words, the pulse width of the axial strain for the monolayer polyurea foam samples shows a significant increase, which is a

Fig. 4 In-plane strain components in the axial (along the impact direction), lateral (orthogonal to the impact direction) directions for conventional monolayer, homogenous density polyurea and benchmark foams as well as bilayer mono-density polyurea foams. The strain components within the interface regions are also plotted for the bilayer samples

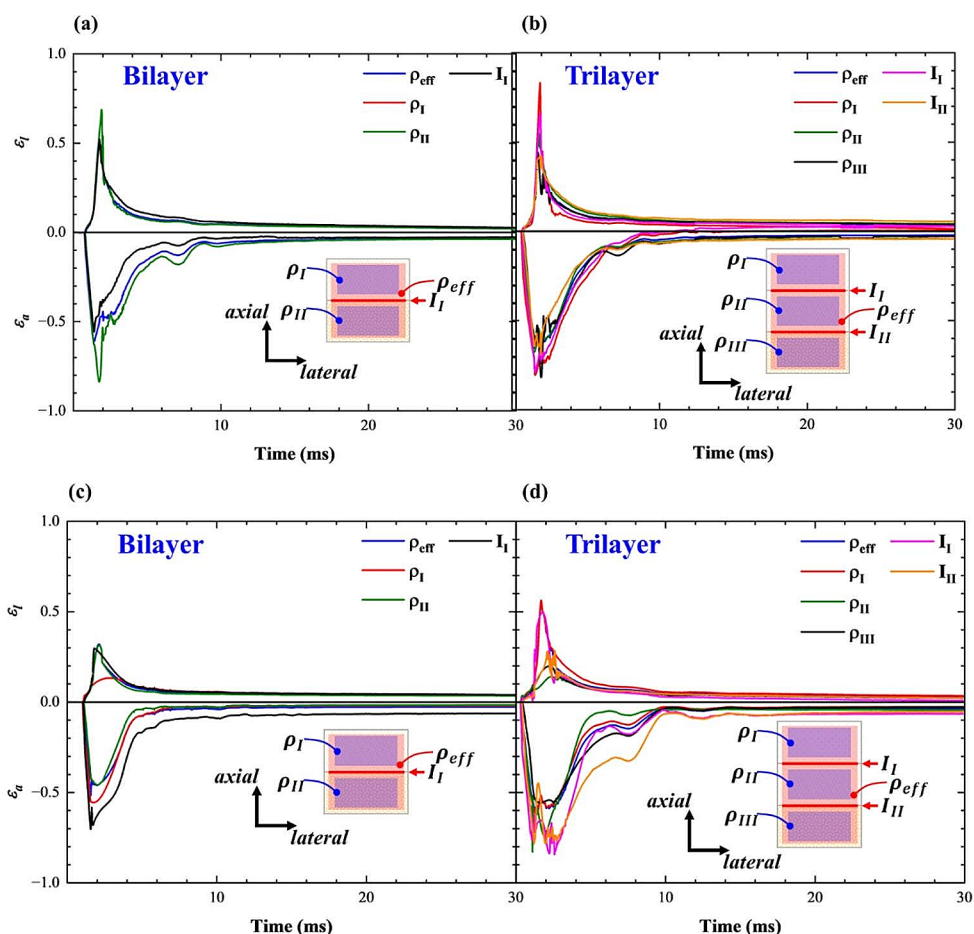


desirable property in protective foams since it improves its hysteretic response and reduces the bluntness of the incoming impact. Finally, the resolved Poisson's ratio based on the in-plane strain components axiomatically shows the rapid transformation of these foams from the behavior of typical cellular solids with low Poisson's ratio (deduced from the graphs upon transformation to true strains) to highly anisotropic structures with large differences between lateral and axial response approaching unity at maximum strains. At the onset of the impact loading ($@\epsilon_a \approx -50mstrain$), the resolved Poisson's ratios for benchmark, monolayer, and seamless mono-density foams are 0.14, 0.08, and 0.14, respectively. Expectedly, the remaining types of foam samples reported Poisson's ratio within the same range.

The axial and lateral strain histories of bilayer and trilayer polyurea foams are plotted in Fig. 5, including the average strain components over the entire sample, the strains within each layer, and the strains within the interface regions. In general, the impact-induced strain in the seamless bilayer (Fig. 5a) and trilayer (Fig. 5b) polyurea foam structures exceeds their adhered counterparts (Fig. 5c and d). For example, the maximum axial strain (calculated over the entire sample) for seamless bilayer and trilayer samples was reported to be $\sim 51\%$ and $\sim 65\%$, respectively, whereas it was $\sim 46\%$ and $\sim 62\%$ for the corresponding adhered samples, from the available DIC analysis. The variation in the reported maximum strains reinforced the previous

discussion about the effect of the interface, where adhered surfaces appear to attenuate the generated strains. In contrast, the seamless interfaces add foundational compliance to preceding layers. The strain-time histories for density-graded polyurea foams also point to four experimental observations. First, the temporal differences between the lateral and the respective axial strain profiles, including the initial lag and terminal recovery, as discussed above, highlight the pronounced time-dependent behavior of polyurea foams. Adding to our previous studies, the mechanical performance of polyurea foams continues to transcend several strain rate regimes, potentially providing efficacy over a broad range of loading scenarios. Second is the temporal spread of the strain-time histories, i.e., pulse duration, which remained nearly unchanged regardless of the number of layers or interface type. The unchanged spread indicates that the microcellular structure and the base material, being the same throughout, dominate the mechanical response, subsiding the influence of the interfacing and gradation strategies. Third, increasing the number of layers in the density-graded structures, i.e., trilayer vs. bilayer, enhanced the generated axial and lateral strains. The induced strains potentially improved impact efficacy by amplifying the strain energy absorption. Future research by this group is keen on studying the dynamic stress-strain response of these foams at the reported strain rate. Finally, fourth is the drastic difference between the rise and decay behavior of the axial

Fig. 5 Strain-time histories for seamless and adhered polyurea foams in bilayer and trilayer graded configurations, demonstrating the hyper-viscoelastic response with excessive deformation and pseudo-anisotropy



strains (also evident in the lateral strain profiles). The strain rise behavior is sharper and steeper than the decay counterpart since the initial speed of the accelerated projectile was reduced due to the energy dissipated during the foam deformation. As discussed, such rise and decay differences also arose from the kinematic boundary conditions as the samples underwent unconfined uniaxial compression.

At the outset, polyurea foams, regardless of their gradation or interfacing strategies, exhibited a peculiar and intriguing response under the examined strain rate loading scenario, which was only evident from the image-based analysis. An indication of this peculiar response was revealed in the strain-time histories presented above, signifying excessive deformation beyond those typically reported at densification for cellular solids [5]. High-speed imaging evidence (Fig. 6) suggests that polyurea foams have undergone pseudo-liquefaction upon densification as the axial strains exceeded 70% and continued to reach maximum strains ca. 90%. That is, polyurea foams completely and rapidly collapse under the projectile upon reaching full densification, behaving like a liquid, i.e., temporary loss of inherent stiffness as the foam samples spread laterally. Figure 7 compares represented foam samples before impact, at maximum deformation (evidencing the reported

pseudo-liquefaction phenomenon), and after the impact event lapsed. At such a point, the viscous properties of polyurea suddenly dominate the mechanical response, dragging the storage and loss moduli along the temperature axis toward the melting point. Shifting of thermal transitions has been previously discussed with respect to the glass transition temperature, e.g., Vogel-Fulcher-Tammann law [40], where the latter roams on the temperature axis as a function of the strain rate [40]. Here, we observe for the first time a similar phenomenon but for the softening regime. This is remarkable! The maximum impact efficacy is associated with high loss modulus in viscoelastic materials, such as polyurea [28, 29, 34], where the loss modulus exemplified the dampening properties [24]. Hence, the momentary transformation of polyurea foams from the rubbery to the pseudo-melt phase (apparent resistance to deformation loss) enhances the potential impact efficacy of this type of elastomeric foam. While the samples were anecdotally observed to be significantly warmer to touch than the starting foam temperature upon impact, the thermocouple placed close the bottom surface of the sample reported a 3.0 ± 0.8 °C. However, it is imperative to note that the thermocouple was not attached to the sample to avoid altering the impact or obscuring the projectile; hence, the thermal changes must be

Fig. 6 High-speed imaging and contour plots from (a) mono-layer, (b) bilayer, and (c) trilayer polyurea foams, showing a pseudo-liquefaction after densification during moderate strain rate impact scenarios

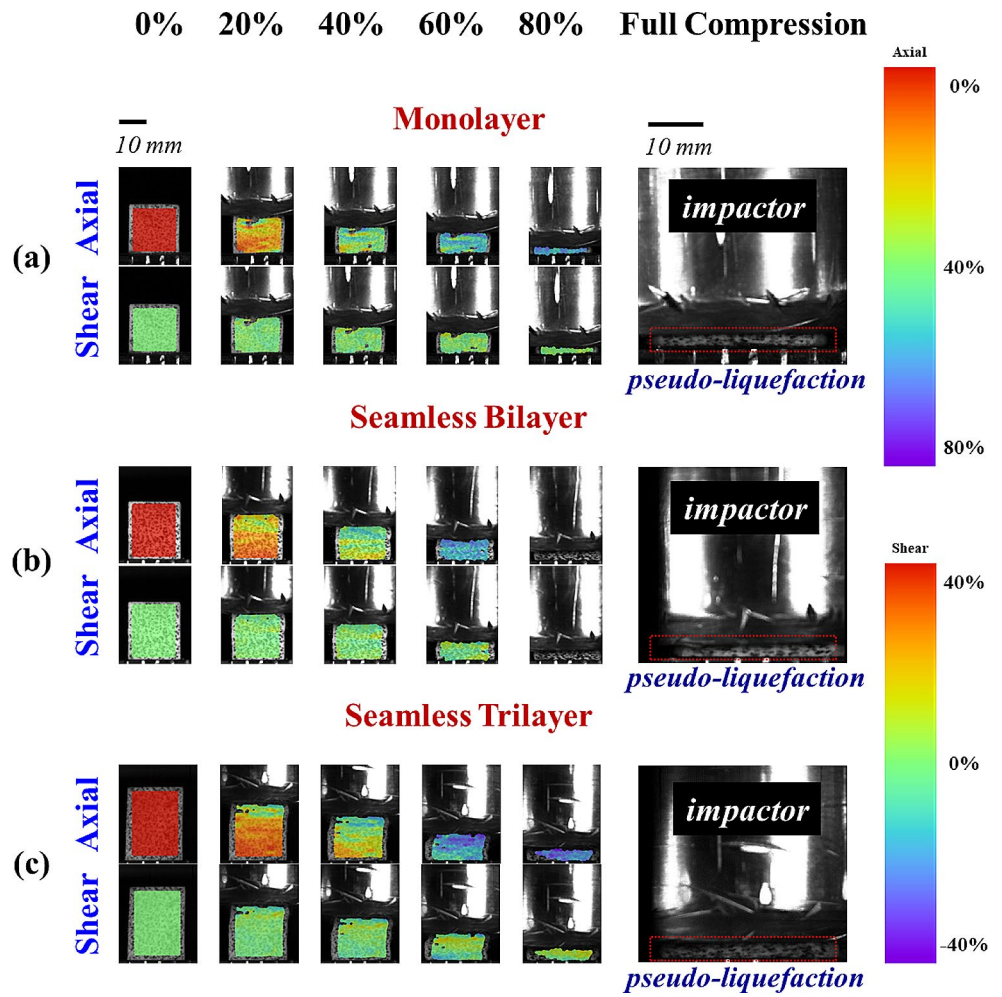
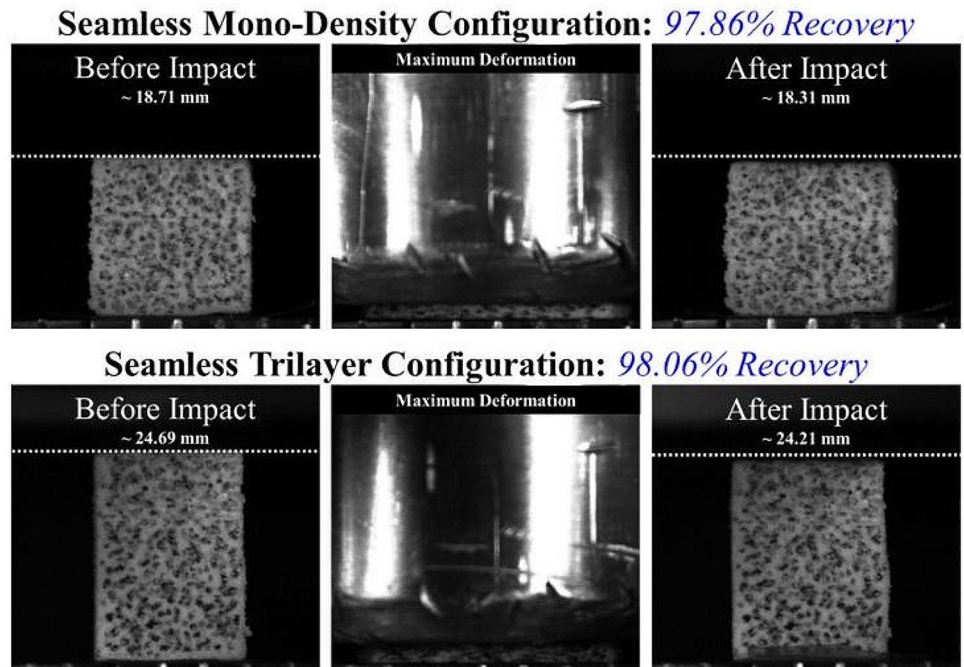


Fig. 7 Representative examples of the polyurea foams during and after the impact events, highlighting the pseudo-liquefaction and recovery behaviors: (a) seamless mono-density and (b) seamless trilayer polyurea foams



further explored in future research. To further substantiate these observations, future research will focus on collecting the companion force-time histories during high strain rate impacts to construct the dynamic stress-strain response and quantify the evolution in the specific absorbed energy, i.e., changes in the impact efficacy as a function of strain rate. Furthermore, thermal cameras will be integrated into the experimental setup to ascertain the changes in temperature as a function of the impact event using noncontact methods to avoid altering the projectile path or the resolved deformations. At the outset, polyurea foams recovered to > 96% of their original heights upon the complete departure of the impacting projectile. Figure 7 shows evidence of the remarkable recovery properties of polyurea foams, showing two representative examples of the recovered seamless mono-density and trilayer samples. The rapid recovery can be viewed in the attached Supplementary Videos. Despite the significant deformation and pseudo-liquefaction phenomenon, this rapid recovery indicates the superior impact performance of polyurea foams while substantiating their prospects for higher efficacy in sports gears and impacting mitigating structures.

Conclusion

This research employed a small-scale shock tube, designed and built in-house, to explore the response of conventional and density-graded polyurea elastomeric foams under moderate-velocity impact loading events with up to 4000 s^{-1} strain rates. The graded polyurea foam samples were extracted from prefabricated sheets with two interfacing strategies, namely (1) seamless interface and (2) adhered interface. Digital image correlation was used to analyze high-speed imaging footage, resolving the strain-time histories in the axial and lateral directions within the overall samples and separately within individual layers. Generally, graded polyurea foams with seamless interfaces exhibited greater compliance than adhered counterparts, illustrated by the significant strains in the first layer of the samples. The axial and lateral strain histories reported in polyurea foams elucidated their hyper-viscoelastic properties, leading to additional energy dissipation mechanisms. Ubiquitously, polyurea foams, irrespective of interfacing and gradation strategies, exemplified lateral strains lagging their axial correspondence, an asymmetric recovery indicating directional anisotropy, and undergoing pseudo-liquefaction (observed herein for the first time) upon densification with strains $\geq 90\%$. The pseudo-liquefaction phenomenon signifies a temporary loss of inherent stiffness, where viscous damping dominates the mechanical behavior. Notably, all polyurea foams tested herein fully recovered during the

unloading phase, reaching ca. 96% of the virgin height. The results of this study have shown the impact mitigating efficacy of polyurea and the considerable advantages of density gradation and interfacing strategies in impact response. The overarching outcome of this research is affirming the impact tolerance of polyurea foams, pointing toward potential higher efficacy under repeated loads.

Supplementary Information The online version contains supplementary material available at <https://doi.org/10.1007/s40870-024-00410-4>.

Acknowledgements The authors acknowledge the support by the National Science Foundation under Grant No. 2035663 (Youssef) and Grant No. 2035660 (Koohbor). The authors are also grateful for internal funding from San Diego State University and Rowan University. The first author was partially funded from San Diego State University's Summer Undergraduate Research Program. Funding from the Department of Defense (G.Y.: W911NF1410039 and W911NF1810477) is also acknowledged. The authors are grateful for the discussion with Ms. Mia Chen during the design of the projectile attachment mechanism.

Declarations

Conflict of Interest The authors have no relevant financial or non-financial interests to disclose.

References

- Koohbor B et al (2022) *Dynamic behavior and impact tolerance of Elastomeric Foams subjected to multiple impact conditions*. J Dynamic Behav Mater.; p. 1–12
- Youssef G et al (2023) Density-dependent impact resilience and auxeticity of Elastomeric Polyurea Foams. Adv Eng Mater 25(1):2200578
- Rahman O et al (2022) Density-graded Cellular solids: mechanics, fabrication, and applications. Adv Eng Mater 24(1):2100646
- Mills N (2007) Polymer foams handbook: engineering and biomechanics applications and design guide. Elsevier
- Gibson LJ (2003) Cellular solids. MRS Bull 28(4):270–274
- Landrock AH (1995) Handbook of plastic foams: types, properties, manufacture and applications. Elsevier
- Chanda M (2017) Plastics technology handbook. CRC press
- Youssef G et al (2020) Experimentally-validated predictions of impact response of polyurea foams using viscoelasticity based on bulk properties. Mech Mater 148:103432
- Smeets M, Koohbor B, Youssef G (2023) Quasi-static mechanical response of density-graded Polyurea Elastomeric foams. ACS Applied Polymer Materials
- Youssef G et al (2022) *Density-dependent impact resilience and auxeticity of Elastomeric Polyurea Foams*. Adv Eng Mater.; p. 2200578
- Ramirez B, Gupta V (2018) Evaluation of novel temperature-stable viscoelastic polyurea foams as helmet liner materials. Mater Design 137:298–304
- Ramirez BJ, Gupta V (2019) Energy absorption and low velocity impact response of open-cell polyurea foams. J Dynamic Behav Mater 5(2):132–142
- Reed N et al (2020) Synthesis and characterization of elastomeric polyurea foam. J Appl Polym Sci 137(26):48839

14. Koohbor B et al (2021) Characterization of energy absorption and strain rate sensitivity of a novel elastomeric polyurea foam. *Adv Eng Mater* 23(1):2000797
15. Ramirez BJ, Gupta V (2019) Energy absorption and low velocity impact response of open-cell polyurea foams. *J Dynamic Behav Mater* 5:132–142
16. Youssef G, Reed N (2021) Scalable manufacturing method of property-tailorable polyurea foam. Google Patents
17. Do S et al (2020) Partially-perforated self-reinforced polyurea foams. *Appl Sci* 10(17):5869
18. Do S, Stepp S, Youssef G (2020) Quasi-static and dynamic characterization of polyurea microspheres reinforced polyurea matrix composite. *Mater Today Commun* 25:101464
19. Uddin KZ et al (2020) Gradient optimization of multi-layered density-graded foam laminates for footwear material design. *J Biomech* 109:109950
20. Do S et al (2022) Thermomechanical investigations of polyurea microspheres. *Polym Bull* 79(2):1081–1095
21. Uddin KZ et al (2022) Tuning the mechanical behavior of density-graded elastomeric foam structures via Interlayer Properties. *ACS omega*
22. Koohbor B, Youssef G (2023) *Polymeric foams and their nano-composite derivatives for shock absorption, in multifunctional polymeric foams*. CRC Press, pp 145–167
23. Smeets M, Koohbor B, Youssef G (2023) The impact efficacy of density-graded Polyurea Elastomeric foams. Unpublished
24. Youssef G (2021) Applied mechanics of polymers: properties, processing, and behavior. Elsevier
25. Siviour CR, Jordan JL (2016) High strain rate mechanics of polymers: a review. *J Dynamic Behav Mater* 2:15–32
26. Ramirez BJ, Gupta V (2019) High tear strength polyurea foams with low compression set and shrinkage properties at elevated temperatures. *Int J Mech Sci* 150:29–34
27. Gupta V et al (2015) Adhesive and ultrahigh strain rate properties of polyurea under tension, tension/shear, and pressure/shear loadings with applications to multilayer armors. *Elastomeric Polym high rate Sensitivity: Appl Blast Shockwave Penetration Mech* 1:71–92
28. Youssef G, Gupta V (2012) Dynamic response of polyurea subjected to nanosecond rise-time stress waves. *Mech Time-Dependent Mater* 16:317–328
29. Youssef G, Gupta V (2012) Dynamic tensile strength of polyurea. *J Mater Res* 27(2):494–499
30. Jain A, Youssef G, Gupta V (2013) Dynamic tensile strength of polyurea-bonded steel/E-glass composite joints. *J Adhes Sci Technol* 27(4):403–412
31. Bhagavathula KB et al (2018) High rate compressive behaviour of a dilatant polymeric foam. *J Dynamic Behav Mater* 4:573–585
32. Koohbor B, Pagliocca N, Youssef G (2021) A multiscale experimental approach to characterize micro-to-macro transition length scale in polymer foams. *Mech Mater* 161:104006
33. Koohbor B, Ravindran S, Kidane A (2021) Situ deformation characterization of density-graded foams in quasi-static and impact loading conditions. *Int J Impact Eng* 150:103820
34. Youssef GH (2011) Dynamic properties of polyurea. University of California, Los Angeles
35. Beranek V, Votapek P, Stastny P (2023) Force and velocity of impact during upper limb strikes in combat sports: a systematic review and meta-analysis. *Sports Biomech* 22(8):921–939
36. Withnall C et al (2005) Biomechanical investigation of head impacts in football. *Br J Sports Med* 39(suppl 1):i49–i57
37. Glazier PS, Mehdizadeh S (2019) Challenging conventional paradigms in applied sports biomechanics research. *Sports Med* 49(2):171–176
38. Cross R (2014) Impact of sports balls with striking implements. *Sports Eng* 17:3–22
39. Wang B, Pan B (2016) Subset-based local vs. finite element-based global digital image correlation: a comparison study. *Theor Appl Mech Lett* 6(5):200–208
40. Ferry JD (1980) Viscoelastic properties of polymers. John Wiley & Sons

Publisher's Note Springer Nature remains neutral with regard to jurisdictional claims in published maps and institutional affiliations.

Springer Nature or its licensor (e.g. a society or other partner) holds exclusive rights to this article under a publishing agreement with the author(s) or other rightsholder(s); author self-archiving of the accepted manuscript version of this article is solely governed by the terms of such publishing agreement and applicable law.